1.1 AN ACOUSTIC DISDROMETER: THE MEASUREMENT OF RAIN KINETIC ENERGY AND RAIN INTENSITY USING AN ACOUSTIC DISDROMETER

Mr. Philip N. Winder[1], Dr. Kevin. S. Paulson

University of Hull, Cottingham Road, Hull, East Yorkshire, HU6 7RX, UK

Abstract

Microwave engineers and geomorphologists require rainfall data with a much greater temporal resolution, and a better representation of the numbers of large raindrops than is available from current commercial instruments. This paper describes an acoustic instrument that determines rain parameters from the sound of raindrops falling into a tank of water. There is a direct relationship between the kinetic energy of a raindrop and the acoustic energy that it creates upon impact. Rain kinetic energy flux density (KE) is estimated from measurements of the sound field in the tank and these have been compared to measurements from a co-sited commercial disdrometer. Six months data has been collected in the Eastern UK. Comparisons of rain KE estimated by the two instruments are presented and links between KR and rainfall intensity (RI) are discussed. The sampling errors of the two instruments are analysed to show that the acoustic instrument can produce rain KE measurements with a one-second integration time with sampling uncertainty of the same size as commercial instruments using a one-minute integration time.

Keywords: Disdrometer, Acoustic disdrometer, Acoustic rain gauge, AWTRG, Acoustic water tank rain gauge, Kinetic energy, Rain rate, Rain intensity, Acoustic intensity, Integration time

1. INTRODUCTION

Rain disdrometers are instruments that determine the distribution of drop sizes present in rain e.g. the Joss-Waldvogel (JW) impact disdrometer or the Thies Laser Precipitation Monitor (LPM). Typically they measure the parameters of individual drops as they impact on, or fall through, a horizontal catchment area or estimate the drop size distribution from empirical relationships. The JW disdrometer deduces drop sizes from drop momentum while the Thies LPM measures the amount of light scattered out of a laser beam. The near simultaneous arrival of two or more drops at the catchment leads to erroneous measurements and so these instruments have small catchments of 25 or 50 cm^2. This limits the instruments to long integration times, typically one minute, and even then the sampling statistics are poor for the large drop tail of the size distribution. The long integration times and poor estimates for the incidence of large drops, means the data from these instruments is inadequate for some applications.

Several applications exist where the effects of rain are highly non-linear with respect to the drop size and which are sensitive to sub-minute rain variation, for example: erosion and radio communications. The scatter of microwaves by rain is important in telecommunications and radar meteorology. At microwave frequencies this is a Rayleigh scattering process where the scatter from a raindrop is proportional to its diameter to the sixth power and so radar reflectivity and microwave specific attenuation are very sensitive to the numbers of large drops. Furthermore, the performance of a microwave telecommunications link is measured using metrics that depends upon the second-to-second variation in bit-error-rate (BER). The BER is related to the total rain fade which is approximately determined by all the raindrops in the first Fresnel zone of the link. This volume is typ-

[1]Author address: Mr. Philip Winder, Dept. Engineering, University of Hull, Cottingham Rd., Hull, East Yorkshire, HU6 7RX, UK. E-Mail: philipwinder@gmail.com

ically of the order of metres across and often only a few hundred metres long. Consequently, the simulation of microwave channels requires high temporal resolution drop size distribution (DSD) measurements with accurate large drop tails Similarly, erosion processes are sensitive to rapid rain variation and are highly non-linear in drop size, (Dijk et al., 2002). Erosivity is a combined function of the rain intensity and of its velocity, so rain kinetic energy flux is often cited as a primary indicator, e.g. (Brodie, Rosewell, 2007; Salles, Poesen, 2000). A large proportion of the kinetic energy is carries by the small proportion of larger drops.

An alternative approach to that used by disdrometers currently on the market is to determine rain parameters from the sound generated from raindrop impacts upon a body of water e.g. (Nystuen (1987); Oguz and Prosperetti (1991); Nystuen et al. (1993); Ma et al. (2005)). The acoustic signal produced by a drop impact can be as short as 40 microseconds and so potentially large numbers of individual impacts can be measured over a short time interval. This allows large catchment areas and short integration times e.g. one second or shorter. Some rain parameters can be deduced from the total sound field, which is much simpler than identifying individual impacts, and this allows even larger catchments and higher temporal resolution. For total sound field measurements these instruments are limited by the quality of amplifying equipment, the number of listening devices and the power in extraneous noise.

All known total sound field measurements have been derived from acoustic rain gauges (ARG) designed for use at sea, where standard instruments are not appropriate. These ARGs are suspended approximately 20 m below the water surface and measure the sound of rain falling on an effective catchment area approximately 60 m across. This is six orders of magnitude larger than the JW or LPM disdrometers and could yield measurements with considerably shorter integration times. The limitations of the method arises from difficulties in distinguishing the sound produced by drops in different size ranges in the total sound field and filtering out other sound sources e.g. waves, wind, ships and animals.

In this paper we describe the development of an acoustic, water tank rain gauge (AWTRG) for use on land. The measurement of total sound field in a water tank removes the majority of noise contamination sources present in marine measurements.

In Section 2 we summarise the processes that convert energy in a raindrop to acoustic energy and the properties of acoustic signals generated by impact of a water drop on a liquid surface. Section 3 describes the design and construction of the AWTRG; both the physical properties of the tank and the signal processing electronics. Section 4 develops algorithms for estimating rain parameters from tank measurements while Section 5 compares tank-derived parameters from those derived from measurements of a cosited LPM. Section 6 provides some conclusions and discussed future work.

2. BACKGROUND

Several studies since 1959 have shown that there are three main sources of sound from a water drop falling on a water surface, each with different temporal character and frequency content, (Medwin et al., 1992; Mani and Pillai, 2004). The impact of raindrops on the water's surface generates a sharp initial pressure rise corresponding to radiated sound of short duration (between 10 and 40 μs) and a damped pressure wave with predominantly low frequency content (below 600 Hz) associated with a near field hydrodynamic effect. Raindrops also cause strongly radiating air bubbles that are formed from several tens to hundreds of milliseconds after the impact. These bubbles oscillate and radiate sound with frequencies of 10-20 kHz for up to 10 ms before reaching a state of equilibrium. In laboratory studies using a 26 m long vertical utilities shaft and an anechoic water tank (a 1.5 m high and 1.5 m diameter cylindrical redwood barrel with a lining of redwood wedges), Medwin et al. (1992), have carried out a comprehensive analysis of the acoustic signatures for drops of different sizes, and have found that the relative proportions of impact and bubble noise vary with drop size. Drops below 0.7 mm in diameter were not heard. Drops with diameters in the range 0.8 to 1.1 mm (associated with drizzle) cause an impulse lasting for less than 10 μs and loud bubble noise across the frequency range 12 to 21 kHz. Typically, drops with diameters in the range 1.1 to 2.2 mm cause loud impact noise but do not create bubbles. Large drops with diameters above 2.2 mm cause very loud impact and bubble noise across the frequency range 1 to 50 kHz, although not all large drops create bubbles. Medwin et al. (1992), derived an empirical relationship between the peak frequency of the bubble noise in the range 12 to 21 kHz and the raindrop volume. Mani and Pillai (2004), have shown that the acoustic signature of the pressure wave associated with raindrop impact on a water surface can be used for drop size measurement.

Figure 2 illustrates an acoustic signal measured by a hydrophone, generated by the impact of a raindrop on a water surface. The signal around 0.2 ms is the impact pulse while the damped ringing from 1.6 ms onwards is due to bubble oscillation. For this illustration, the time interval between impact and bubble noise has been reduced for clarity. Typical durations are between 1 and 500 ms. The bubble noise is a serious problem when attempting to invert the acoustic signal generated by rain falling into water to yield rain parameters. It increases the duration of the acoustic signal generated by a drop impact from as short as 10 μs to as long as 0.5 seconds. This greatly reduces the rate at which individual drop signals can be generated before they overlap. Furthermore, the bubble noise is often of higher amplitude than the impact pulse. Potentially this can lead to bubble noise being interpreted as multiple drop impacts. The bubble noise produced by a specific drop is also highly variable and depends upon parameters we cannot measure, such as impact angle and the internal hydrodynamics of the drop, e.g. see Medwin et al. (1990).

Regular entrainment, (Franz, 2002; Pumphrey and Crum, 1989), refers to the process where a bubble is created repeatedly when a droplet impacts on the surface of a liquid, usually water. Several studies developed the mechanics of entrainment, (Prosperetti and Oguz, 1993), and found that there are a several scenarios when entrainment can occur. Regular entrainment occurs when a crater is formed in the water after an impact. As the liquid returns to its equilibrium and since the drop is still forcing the surface of the liquid downwards the sides of the crater can collapse, or 'pinch-off' due to a travelling capillary wave. The resulting void at the bottom part of the crater forms a bubble. Drop shape is determined by the internal hydro-dynamics and the air drag. Large drops are approximately oblate spheroids and very large drops become concave on the bottom. When a large drop impacts the preceding air is forced into the water which develops into an "azimuthal necklace", (Thoroddsen et al., 2003). Surface tension breaks up the necklace into a ring of stable bubbles. The third type of entrainment is formed when, after an initial large impact, further smaller droplets are ejected from the impact site and create their own bubbles via the first two entrainment processes. This can be due to funnel formation and separation from a crater collapse or from a crown formation ejecting droplets into the air when a crater is formed with a very large energy impact. Irrespective of the type of entrainment, the resultant bubble will be suspect to the comparatively large pressure of being underwater. This will compress the bubble until a point where its surface tension is greater than the force exerted on the bubble. The bubble will then expand again oscillating until the two pressures reach equilibrium. Because the entrained air is not spherical, there will also be spherical harmonic oscillations until it regains spherical equilibrium.

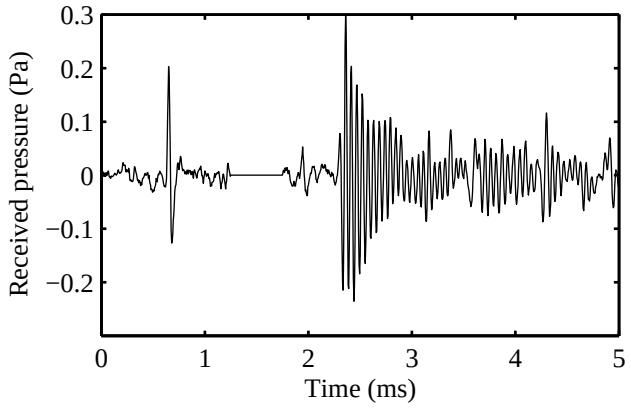

Figure 1: A typical measured droplet impact and bubble signal using the AWTRG.

The effect of wind has been investigated by Medwin et al. (1990). Falling raindrops are advected horizontally by the wind resulting in oblique incidence on the water surface. As a consequence, the probability of bubble production is altered and the amount of energy in the impact pulse changes. They found that with an increasing wind speed, the resultant spectrum of the rain alters. As the angle of incidence increases, less bubbles are created and their contribution to the spectra becomes weaker and changes to a higher frequency. At the same time, the contribution to the spectrum from the broadband impact signal becomes stronger.

Many researchers have reported the acoustic spectra of the total sound field produced by natural rain falling into water e.g. (Lavile et al., 1991; Medwin et al., 1992; Nystuen et al., 1993; Pumphrey and Crum, 1989). These studies found that most rain events yielded a spectral peak at around 14-16 kHz, principally generated by bubble oscillation. The rest of the spectrum is created by the impact signal, and since it is impulse-like in time, the corresponding spectrum is broadband in nature; although it reduces as the frequency increases due

to the finite pulse duration.

Originally it was planned to suppress all bubble production by the addition of a surfactant, in order to derive relationships that were independent of bubble noise. Pumphrey and Crum (1989) stated that if the water surface tension was reduced below 30 dyn/cm, the production of entrained bubbles was eliminated. Experimentally it was found that the addition of surfactants to decrease the surface tension would promote the formation of bubbles on the surface of the water . These bubbles would then cushion subsequent drops and eventually burst resulting in another high amplitude signal. It was found that a 1 cm thick layer of cooking oil floating on the water surface suppressed bubble production since the viscosity of the oil reduced the size of crater formation to the point where it would not pinch off and create a bubble. This has been confirmed by recent work by Deng et al. (2007), who formulated the idea of a capillary number; the ratio between the viscosity and the surface tension. However, oil was not suitable for a rain measurement instrument as heavy rain lead to pools of water on the oil surface and the oil was not stable for long period due to the growth of algae and bacteria.

As we have not found a way of suppressing bubble noise, rain parameter estimation algorithms need to be consistent with typical bubble noise production.

3. THE ACOUSTIC WATER TANK RAIN GAUGE

Data was collected in a water-filled, cylindrical plastic tank, with a cross-sectional area of 0.38 m^2 and a depth of 0.5 m. The tank was lined with a combination of natural rubber and foam to form a semi-anechoic lining with an attenuation coefficient of approximately 0.5 at 50 kHz. The purpose of the lining is to reduce the duration of the impulse response for each drop impact. Four SRD HS/150 omnidirectional hydrophones were fixed to the inside, bottom of the tank near the edge in the compass directions. Each hydrophone is connected to a proprietary charge amplifier designed to optimise the dynamic range. The amplified signal is sampled at 200 kilo samples per second (ksps), with 24-bit resolution, using a PC hosted NI-4462 data acquisition card. The measurements are archived by the PC.

A Thies Clima Laser Precipitation Monitor (LPM) is sited within 0.5 m of the tank edge and at the same level as the water surface. Both instruments are installed in a suburban garden in Hull, UK [53.76735,-0.366345]. The instruments are approximately 10 m from the southern aspect of a two-storey house and there are trees over 20 m tall approximately 50 m from the instruments. Although the situation is far from ideal for accurate rain parameter measurements, due to disturbance of the wind field by the buildings and trees, we are interested in comparing parameters estimated from the LPM and the acoustic measurements made in the tank. It is reasonable to expect the two instruments to experience the same rain parameters.

The LPM is operated in event mode where the diameter and fall-speed of each drop is recorded. This allows DSD and related parameters to be calculated with a range of integration periods. A large amount of data is produced and this will overwhelm the serial data connection at rain intensitys in excess of 100 mm/hr.

4. COMPARISON OF MEASUREMENTS

Over a period of three months beginning in October 2009, rain events were observed with simultaneous recording of the sound field in the water tank at the four hydrophones and the drops arriving at the LPM. The objective was to determine what rain parameters, at what temporal resolution, could be derived from the acoustic measurements. Both instruments yield measurements affected by a range of systematic and random errors. When comparing measurements it is important to understand what differences are significant. The largest uncertainty is introduced by the relatively small sample volume of the LPM i.e. the drops recorded by the LPM are unlikely to be representative of the DSD in the atmosphere above the instruments. In the paragraphs below we derive expressions for the uncertainty in measured rain parameters in terms of the instrument sample volumes.

4.1. Sampling errors in measured rain parameters

Rain measurements typically derive rain parameters from the raindrops in a sample volume of atmosphere e.g. meteorological radar; or the raindrops that cross a horizontal catchment area in an interval of time e.g. a rain gauge or disdrometer. The raindrops in the sample will have different sizes and relative positions each time a measurement is performed, even if the notional rain parameter e.g. rain intensity or rain kinetic energy, is constant. This yields a temporal fluctuation in the measured parameter around the notional value and a spread of likely measured values characterized by a variance.

The numbers and relative positions of raindrops in the atmosphere are determined by very complex processes including coalescence and break-up, along with evaporation and turbulent inertial sorting. Although this leads to some clustering, drop arrivals at a catchment is often modelled as a Poisson process.

The distribution of drops over some small diameter range i.e. , can be modelled as Poisson as drops of a particular size are likely to have been produced by different, and uncorrelated, break-up events. The same arguments hold for the arrival of raindrops at an instrument catchment area. This has been experimentally verified by Joss and Waldvogel, (1969). If we assume that the arrival of drops in a small size interval is a Poisson process, this allows the calculation of the variation in rain parameters derived from DSD measurements over a range of integration intervals. The Poisson distribution is discrete and has the property that the mean is equal to the variance.

4.2. Sample Errors in Catchment Rain Measurements

Instruments such as rain gauges and disdrometers measure rain parameters from the raindrops that cross a catchment area A in an integration time T. These instruments can be thought of as sampling a prism of atmosphere above the instrument with cross-section A and height V(D)T. This sample volume is larger for larger raindrops with more rapid fall-speed. This is an advantage for disdrometers as a higher proportion of large drops are measured, compared to a volume sampling instrument, yielding better sampling statistics at the large diameter tail of the DSD. If a horizontal wind is present, the sample prisms are no longer perpendicular to A, but have the same volume.

Consider a rain event with a uniform mean rain intensity of mm/hr. If the sizes of raindrops are Marshall-Palmer distributed then the mean number of drops per unit volume, in the diameter interval , is given by , where is a constant and is a function of the mean rain intensity. The mean number of drops in each size range, measured by the disdrometer is:

$$N_{disd}(D)dD = ATV(D)N(D)dD \tag{1}$$

Where $N_{disd}(D)$ is the observed DSD and $V(D)$ is the fall-speed. Due to the Poisson assumption, the variance of this measurement is:

$$\begin{aligned} Var(N_{disd}(D)dD) &= N_{disd}(D)dD \\ &= ATV(D)N(D)dD \end{aligned} \tag{2}$$

The best estimate of derived from the disdrometer measurement is:

$$N(D)dD \cong \frac{\frac{N_{disd}(D)dD}{ATV(D)}}{\pm\sqrt{\frac{N(D)dD}{ATV(D)}}} \tag{3}$$

It is clear that diameter ranges with small numbers of measured drops yield poor estimates of the number density of these drops in the atmosphere e.g. a bin with 10 measured drops yields an atmospheric number density with a 30% relative error. Note that from equation 3 the variance is inversely proportional to the catchment area of the instrument and the measurement integration time. The AWTRG has a catchment area approximately 85 times larger than the Theis LPM and so would yield rain intensity estimates with the same standard error using an integration time 85 times shorter.

4.3. Comparison of Tank and LPM Rain Kinetic Energy Intensity

The majority of the kinetic energy (KE) of the raindrops landing on a water surface is transformed into acoustic energy, in a fraction of a second, by a range of processes. Measurement of acoustic energy allows estimation of the rain KE flux density i.e. the rate that raindrops falling through a horizontal surface transport KE, (Steiner and Smith, 2000). The KE intensity due to drops of diameter D is:

$$I_{KE}(D) = \frac{1}{AT}KE(D)N_{disd}(D)dD \tag{4}$$

Where $KE(D) = 1/2\,\rho Vol(D)V^2(D)$ is the kinetic energy of a drop of diameter D. The variance in the KE flux density estimate is:

$$Var(I_{KE}) = \frac{1}{(AT)^2}\int_0^{\inf} KE^2(D)N_{disd}(D)dD \tag{5}$$

Writing equation 5 in terms of the atmospheric DSD, as in 3, concludes that the variance due to sampling error is inversely proportional to both catchment area and integration time.

The LPM estimates the vertical component of drop velocity from the amount of light scattered out of a horizontal beam, and the duration of the scattering. Horizontal movement is not detected. The KE of drops moving horizontally with the wind have higher KE than drops falling vertically. If drops are moving with a wind speed W, then the KE is increased to:

$$KE(D,W) = \frac{1}{2}\rho Vol(D)(V^2(D) + W^2) \tag{6}$$

For moderate wind speeds around 5 ms $^{-1}$, this doubles the KE of drops of diameter 1.3 mm and greatly increase the KE of smaller drops.. This KE will be measured by the tank disdrometer, but not detected by the LPM.

4.4. Rain Kinetic Energy Flux

Almost all the raindrop kinetic energy is converted to acoustic energy within a second of impact on the water surface by a range of mechanisms. The impact pulse and entrained bubble noise, due to the primary impact and splash products, carry the bulk of the energy while much smaller amounts generate surface waves, atmospheric sound and splash products that fall outside the tank. It is reasonable to assume that the acoustic energy measured in the tank over a second or longer would be very close to the kinetic energy carried by the raindrops falling onto the water surface. This hypothesis was tested by comparing one minute, raindrop kinetic energy accumulations estimated using the drops measured by the LPM, with the total acoustic energy measured by the tank hydrophones. Figure 4.4 is the scatter plot of these two quantities with error bars indicating the standard deviations of LPM derived rain kinetic energy flux density calculated using equation 5 and 6. The measured acoustic energy needs to be adjusted at low rain intensities to remove the noise inherent in the measurement electronics. As the system noise and rain generated signal are uncorrelated, the total measured acoustic energy is the sum of noise plus signal energies. The acoustic energy used in Figure 4.4 is the measured acoustic energy minus the energy measured during periods without rain.

The kinetic energy of falling drops needs to be corrected for horizontal movement with the wind. Even for low wind speeds of several meters per second, a large proportion of raindrops would be moving horizontally faster than they are falling. Wind speed was not measured and so Figure 2 uses events where the wind speed was observed to be low. However, the kinetic energy derived from LPM measurements is expected to be an under-estimate. This underestimation will be more significant at lower rain rates where more drop kinetic energy is due to horizontal movement. For this reason the points deviate further from the regression line than due to sampling errors alone and more for low energy flux densities.

4.5. Data Resolution

The AWTRG has a much larger catchment area than the LPM and so, for the same integration time, it yields estimates of rain parameters with a smaller error. Alternatively, it yields estimates of rain parameters with the same precision as the LPM with a much shorter integration time. Consider estimates of kinetic energy flux density from an instrument with catchment area A and integration time T. We can estimate the variance using equation 5.

For the notional case of a uniform mean DSD, the integral in (5) is a constant and the variance in the estimate of kinetic energy flux is inversely proportional to the product of A and T. The tank area is approximately 85 times the LPM catchment and so the standard deviation is approximately a ninth of that provided by the LPM for the same integration time. The AWTRG provides kinetic energy flux estimates with the same variance and standard error with an integration time 1/85th of that of the LPM.

Consider a period of experimental data with a near-constant KE over an integration period of 1 minute. For shorter intervals during this minute, by (5) the expected square deviation of flux density or rain intensity from the average value would be expected to be inversely proportional to the interval length .

From section 4.3 the KE calculations are highly dependent on the velocity of the raindrop. The slight offset within the experimental data in the KE variance is likely due to a non-zero wind speed around the measurement site. The RI is not as dependent on the advection speed, so the theoretical model of (4) is adequate. Despite the dependence on the wind velocity, the principle that the variance is proportional to the integration time still holds. Hence, neglecting any noise arising from external or electronic sources in both instruments, the AWTRG with an integration time of 0.7 s can deliver data as accurate as the LPM using one-minute integration times.

5. RESULTS AND DISCUSSION

Over 2 months worth of rainfall data, where the maximum rain intensity of an event was greater than 1 mm/h, were collected during October and December 2009 to compare the AWTRG?s acoustic intensity to the LPM?s kinetic energy readings. From section 4.3, a relationship exists between the KE of the impacting drops and the total sound field. To prove this relationship a suitable sum of the spectra of the AWTRG was chosen between 1-50 kHz to remove any unnecessary and noisy parts of the spectrum. Another option was to monitor an individual frequency bin similar to the work of Ma et al. (2005), and Nystuen (2001), in which a slight improvement in terms of its variance

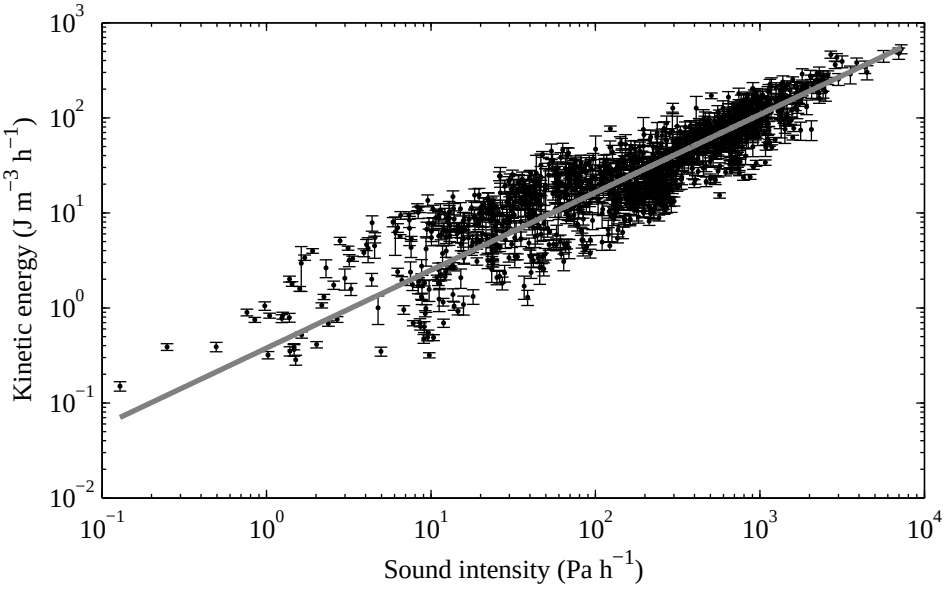

Figure 2: A comparison of LPM derived raindrop kinetic energy flux density with total acoustic energy integrated over one minute. The error bars indicate uncertainty due to sampling errors and the linear regression line is in grey.

was found at 2.8 kHz for the KE and 1.5 kHz for the RI. Ma used the energy at 5 kHz, indicating that the optimal frequency is dependent on operating conditions. Figure **??** is a plot of the collected data showing the relationship. The relationship between the two is clear on a log-log plot, indicating a power law fit. Using least squares regression (LAR method) the following parameters were found to fit the data:

$$y = 0.3778x^{0}.819 \tag{7}$$

After linearising using equation 7, the correlation coefficient is found to be 0.92.

By negating the acoustic intensity data by the intensity with no rain, a noise floor is indicated. From the regression in Figure **??**, a noise floor can be seen in the AWTRG data, which occurs at kinetic energy of approximately 0.07 J; although this value is also affected by the variance. This is due to inherent noise from the electronic circuitry coupled with any external interference. From equation 6 it can be seen that the wind speed greatly affects the kinetic energy, and hence the acoustic intensity. This manifests in the data by increasing the variance since no discrimination between event wind speeds has been made. The remaining variance can be attributed to the random nature of DSD parameters (see equation 2). Further logarithmic relationships between the RI and the KE and the natural fluctuations dependent on the type of event have been reviewed by Salles et al. (2002).

Figure 5 shows an example rain event in time (1 minute integration time) which compares readings from the LPM with that from the AWTRG calculated with equation 7. A similar process can be performed for the laser disdrometer's rain intensity which has a slightly lower correlation coefficient, (0.90) (c.f. Figure

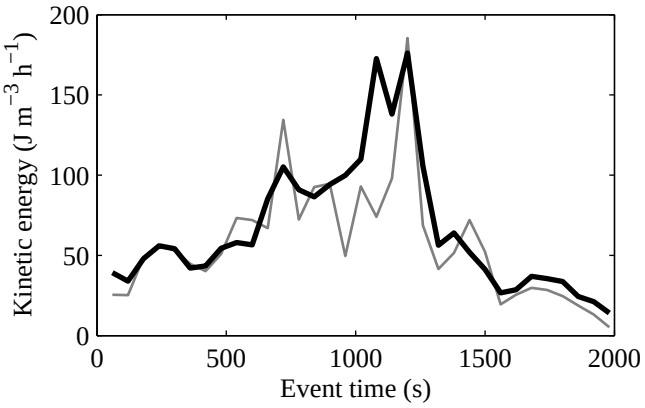

Figure 3: An example rain event comparing the measured KE between the LPM (grey) and AWTRG (black).

5), which yields the following parameters:

$$y = 0.0715x^{0}.6411 \quad (8)$$

Again, a noise floor can be seen within the data which corresponds to 0.02 neglecting the variance. Since the change in wind speed has little effect on the RI (see section 4.3) the majority of the variance is caused by the variability in DSD parameters. Figure 5 shows the RI for the same example event as Figure 5. Nystuen (2001), measures the relative performance of different disdrometers by the means of a correlation coefficient. The coefficients range from 0.79 to 0.94 indicating that both the KE and RI conversions perform at least as well as other disdrometers.

Section 4 established that it is feasible to increase the temporal resolution of the data to below 1 second. Using this information as a verification, an example rain event can be examined (using parameters derived from the minute-long integration data) in Figure **??** to 5. The data has been reduced to 10 and 1 second intervals with the original 60 second laser disdrometer data overlaid for comparison (circles). The data in the 1 second plots (c.f. Figure **??** and 5) show that once the resolution is high enough, short term variations in the kinetic energy and the rain intensity are clearly visible.

6. CONCLUSIONS

The relationship between sound intensity and droplet kinetic energy has been studied experimentally to find the two are correlated, to the point which accurate predictions of the KE and RI are possible from the total sound field. The correlation coefficients obtained perform adequately when compared to other disdrometers. To further improve this relationship, real time sub-second wind data is to be integrated into the AWTRG to reduce the adverse effect where the wind increases a rain drop's velocity to something other than its terminal velocity.

From the results it can be seen that the instantaneous values of KE and RI can be much higher than any disdrometer with a one minute integration time describes, which ultimately affects soil erosion rates and possible communication link downtime. It also shows that there are periods where the RI is much lower than anticipated, at least for a short time. For example, using this information a link?s transmit power could be reduced for this period to save energy reduce costs, and increased to improve reliability. The reliability of this temporal reduction has been rigorously proven to be dependent on the catchment area; hence the results are at least as accurate as comparable commercial disdrometers at a fraction of the integration time.

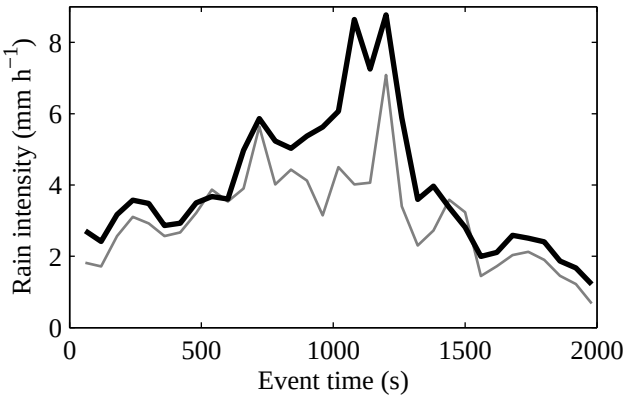

Figure 5: An example rain event comparing the RI between the LPM (grey) and AWTRG (black).

7. REFERENCES

Brodie, I., Rosewell, C., 2007. Theoretical relationships between rainfall intensity and kinetic energy variants associated with stormwater particle washoff. J. Hydrol. 340, 40-47.

Deng, Q., Anilkumar, A.V., Wang, T.G., 2007. The role of viscosity and surface tension in bubble entrapment during drop impact onto a deep liquid pool. J. Fluid Mech. 578, 119-138.

Dijk, A.I.J.M. Van, Bruijnzeel, L.A., Rosewell, C.J, 2002. Rainfall intensity-kinetic energy relationships: a critical literature appraisal. J. Hydrol. 261, 1-23.

Franz, G.J, 1959. Splashes as a source of sound in liquids. J. Acoust. Soc. Am. 31, 1080-1096.

Joss, J., Waldvogel, A., 1969. Raindrop Size Distribution and Sampling Size Errors. J. Atmos. Sci. 26(3), 566-569.

Lavile, F., Abbott, G.D., Miller, M.J., 1991. Underwater sound generation by rainfall. J. Acoust. Soc. Am. 89, 715-721.

Leighton, T.G, 1997. The Acoustic Bubble, Academic Press, London.

Ma, B.B., Nystuen, J.A., Lien, R.J., 2005. Prediction of underwater sound levels from rain and wind. J. Acoust. Soc. Am. 117, 3555-3565.

Mani, T.K., Pillai, P.R.S., 2004. Drop parameter estimation from underwater noise produced by raindrop impact. Acoust. Res. Lett. Online 5(3), 118-124.

Marshall, J.S., Palmer, W.M., 1948. The distribution of raindrops with size. J. Atmos. Sci. 5, 165-166.

Medwin, H., Kurgan, A., Nystuen, J.A., 1990. Impact and bubble sound from raindrops at normal and oblique incidence. J. Acoust. Soc. Am. 88, 413-418.

Medwin, H., Nystuen, J.A., Jacobus, P.W., Ostwald, L.H., 1992. The anatomy of underwater rain noise. J. Acoust. Soc. Am. 92, 1613-1623.

Nystuen, J.A., 1987. Rainfall measurements using underwater ambient noise. J. Acoust. Soc. Am. 79, 972-982.

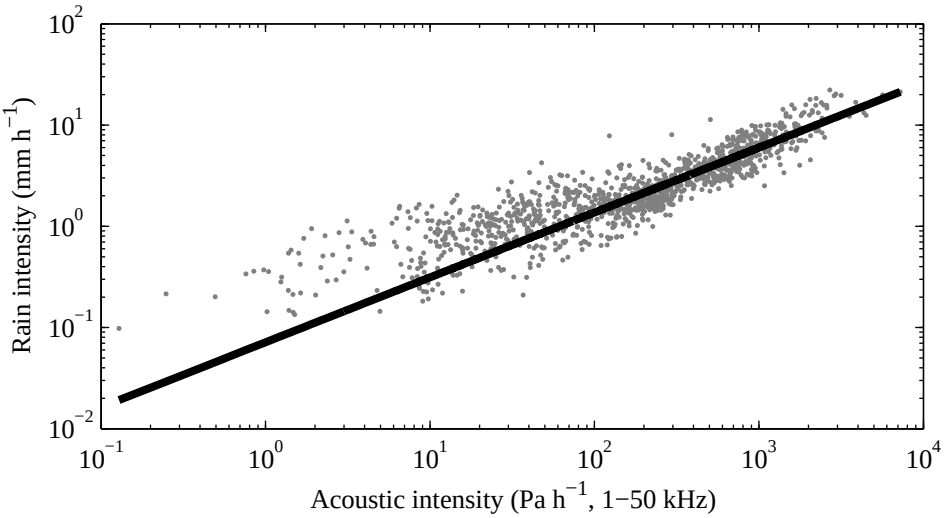

Figure 4: The relationship between total acoustic intensity and rain intensity. As Figure **??**.

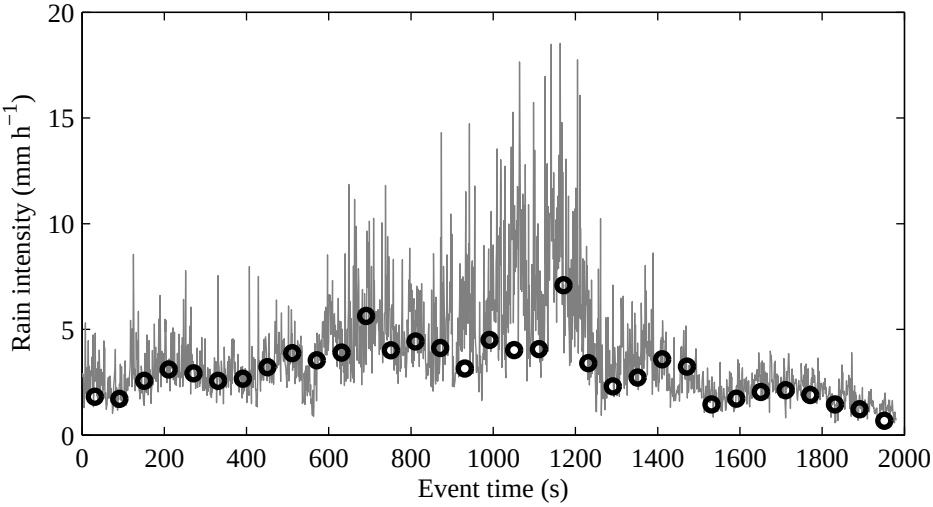

Figure 6: : Typical rain intensity data. The AWTRG data, (line), are reduced to 1 second integration times.

Nystuen, J.A., McGlothin, C.C., Cook, M.S., 1993. The underwater sound generated by heavy rainfall. J. Acoust. Soc. Am. 93, 3169-3177.

Nystuen, J.A., 2001. Listening to raindrops from underwater: an acoustic disdrometer. J. Atmos. Oceanic Technol. 18, 1640-1657.

Oguz, H.N., Prosperetti, A., 1991. Numerical calculation of the underwater noise of rain. J. Fluid Mech. 228, 417-442.

Onof, C., Chandler, R.E., Kakou, A., Northrop, P., Wheater, H.S., Isham, V., 2000. Rainfall modelling using Poisson-cluster processes: a review of developments. J. Stoch. Environ. Res. Risk Assess. 14, 384-411.

Prosperetti, A., Oguz, H.N., 1993. The impact of drops on liquid surfaces and the underwater noise of rain. Annu. Rev. Fluid Mech. 25, 577-602.

Pumphrey, H.C., Crum, L.A., 1989. Underwater sound produced by individual drop impacts and rainfall. J. Acoust. Soc. Am. 85, 1518-1526.

Salles, C., Poesen, J., 2000. Rain properties controlling soil splash detachment. Hydrol. Processes 14, 271-282.

Salles, C., Poesen, J., Sempere-Torres, D., 2002. Kinetic energy of rain and its functional relationship with intensity. J. Hydrol. 257, 256-270.

Steiner, M., Smith, J. A., 2000. Reflectivity, rain rate and kinetic energy flux, relationships based on raindrop spectra, J. Appl. Meteorol. 39(11), 1923-1940.

Thoroddsen, S.T., Etoh, T.G., Takehara, K., 2003. Air entrapment under an impacting drop. J. Fluid Mech. 478, 125-134.